ORIGINAL PAPER

Physical simulation of mining effect caused by a fault tectonic

Pu Wang[1,2] · Lishuai Jiang[3] · Xiaoyu Li[3] · Guangpeng Qin[1,2] · Eryu Wang[4]

Abstract

Due to faults occurring universally and being harmful to coal production, the study of mining effects on faults is significant for predicting rock bursts in coalmines. In this paper, a physical simulation test is conducted, which can intuitively recreate the macroscopic movement of overlying strata. Then, mining effects on fault activation slipping and the responses of abutment stress of coal body and fault plane are studied. The results demonstrate that fault activates and aggravates gradually prior to passing, which leads to abutment stress in the footwall coal rise. This causes the footwall strata to move, and this displacement is large. After just passing the fault, the hanging wall strata slip along the fault plane, which can lead to increasing abutment stress of the hanging wall coal; however, the hanging wall strata move slightly, and this displacement is relatively small. Hence, the fault can be activated and slip prominently in a fault-affected zone, thereby easily inducing rock bursts. Finally, a field case regarding microseismic monitoring is used to verify the simulation results; these can serve as a reference for predicting rock bursts and their classification into hazardous areas under similar conditions.

Keywords Physical simulation · Mining effect · Fault tectonic · Fault slipping · Rock burst

Introduction

Faults, as common geological structures in coalmines, are a geological factor that cannot be ignored in underground mining, and they represent a significant threat to safe coal production (Wang et al. 2018). In Chinese coalmines, fault structures are mainly simple, with small or medium-sized fall heights

✉ Pu Wang
  15854848872@163.com

✉ Lishuai Jiang
  skwp0701@hotmail.com

1 Department of Resources and Civil Engineering, Shandong University of Science and Technology, Tai'an 271019, China

2 National Engineering Laboratory for Coalmine Backfilling Mining, Shandong University of Science and Technology, Tai'an 271019, China

3 State Key Laboratory of Mining Disaster Prevention and Control Co–founded by Shandong Province and the Ministry of Science and Technology, Shandong University of Science and Technology, Qingdao 266590, China

4 State Key Laboratory of Geomechanics & Deep Underground Engineering, China University of Mining & Technology, Beijing 100083, China

(Jiang et al. 2017). Field practices show that fault structures directly or indirectly control inducing rock bursts. Moreover, according to the statistics, more than 70% of accidents occur near faults. For instance, approximately 90% of rock burst accidents every year occur near faults in Laohutai coalmine. Further, in 50 rock burst accidents in Longfeng coalmine, a total of 36 times were statistically found to be directly related to faults. Hence, as mining depth and intensity increase, the frequency and intensity of rock bursts affected by faults rise; this results in ejection of rocks and coal, damage of supports, titling of devices, and even fatalities (Wang et al. 2016; Jiang et al. 2017). Figure 1 shows several field images captured after these accidents.

Commonly used study methods to solve the scientific problems of underground engineering are laboratory tests, field monitoring, theoretical analysis, numerical simulations, and physical simulations. For instance, a true triaxial test was carried out to analyze the two kinds of potential fault plane models (Gong et al. 2015). Microseismic monitoring in the field was used to study the relationship between rock bursts and in situ stress (Xia et al. 2016). The voussoir beam model (through theoretical analysis) was established to study the instability of fault coal pillars (Li et al. 2016); the in situ stress distribution affected by faults is studied by using ADINA software and UDEC software (He et al. 2010; Jiang et al.

Fig. 1 Field images captured after accidents

2018). The fault characteristic parameters and roof physical-mechanical parameters were studied by FLAC2D software and FLAC3D software (Li et al. 2008; Sainoki and Mitri 2015). Roof stability of tunnels or roadways in underground mines was studied with 3DEC software (Shreedharan and Kulatilake 2016; Sherizadeh and Kulatilake 2016; Xing et al. 2018a, b); the laws of stratum behavior and fault slipping were studied using physical simulation tests (Lai et al. 2016; Wang et al. 2014a).

In this paper, the physical simulation test method, which can intuitively recreate and artificially change the testing conditions, is chosen and used to simulate a progressive mining operation. This is because the evolution of deformation and movement and stress of overlying strata are often hidden and inaccessible. This method has many advantages, including being an easy to operate, clear, intuitive, and repeatable test; moreover, it also can ameliorate the disadvantages of field observation and theoretical analysis, such as high cost and time consumption.

Considerable studies regarding physical simulation tests within a fault occurrence have been conducted. For instance, Wang et al. (2017), Peng et al. (2013), and Liu et al. (2011) studied the failure and stress distribution of overlying strata affected by a fault. They obtained the roof caving height and concentrated stress of the coal body (which were large), with the footwall face advancing toward the fault. Dou et al. (2017) tested roadway deformation with and without tectonic stress, finding that the tectonic stress field had a significant effect on roadway deformation failure, which can provide a technical reference for the optimization of roadway layouts. Wang et al. (2014b), Jiang et al. (2013), and Bornyakov et al. (2016) studied the evolution of fault plane stress during the fault slipping process, and deduced that the fault activates more easily when the working face approaches the fault. Wu et al. (2007) studied the mining effect of fault zone rocks and obtained the different response characteristics between the two fault walls. Zuo et al. (2009) monitored roof horizontal displacement through theodolite, and confirmed that slip dislocation occurs near faults based on the monitoring results of the digital speckle correlation and discontinuous deformation methods. Zhang et al. (2015, 2017) developed a new similar solid–fluid

coupling material and conducted a feasibility analysis of the simulated materials to study the expansion activation of concealed faults.

Previous studies were either confined to the laws of mine pressure with fault occurrences or only to the development of similar materials. However, the relationship among the movement of overlying strata, fault activation slipping, and rock bursts near faults has rarely been reported. Hence, in this paper, a physical model test with a working face passing through the fault is carried out; then, the mining effects on fault activation slipping, and the responses of abutment stress of coal body and fault plane stress during the process of fault slipping, are studied. Consequently, the relationship among mining operation, fault activation slipping, and rock bursts near faults is analyzed. Results can serve as a reference for predicting rock bursts, and their classification into hazardous areas under similar conditions.

Scheme of physical simulation test

By using existing equipment in a laboratory and study targets, a two-dimensional model frame with dimensions of 3000 (length) × 400 (width) × 1800 mm (height) was chosen, and a physical model was established based on the similarity theory (Wang et al. 2015a, b; Xuan and Xu 2017; Xia et al. 2017). Then, the similarity ratios (geometry, density, and strength) between the physical model and the prototype were determined as 1/200, 1/1.5, and 1/300, respectively, by considering the study scheme and referring to previous studies (Lai et al. 2016; Xie et al. 2016; Dai et al. 2010).

To create the physical model, similar materials (river sand, calcium carbonate, and gypsum) were applied (Wang et al. 2017). The simulation of different strata in a prototype should be distinguished by different proportions of the materials; this is termed the material ratio, and it is conventionally determined by several uniaxial compressive tests of rock specimens, with each group of specimens being repeatedly tested and compared. Finally, the material ratio was determined by

referring to the literature (Li 1988) and previous test experiences. In addition, mica powder was used to simulate the stratification of rock layers by evenly paving between strata. The prototype strata were derived from the Yangliu coalmine in district 104. Properties of the prototype and physical models, and the material ratios, are listed in Table 1.

The physical model can be deployed by using the similar materials, and the procedure can be divided into six steps: material weighing, material mixing, blending evenly, adding water and mixing evenly, paving and ramming, and removing redundant material. Finally, total height of 1460 mm and roof height of 1100 mm were achieved. However, the physical model cannot fully simulate all strata of the prototype (mining depth of 270 m), and the remaining roof strata in the prototype were compensated by 500 kg iron weights on the physical model. Considering the weak characteristics of a fault, mica powder with a thickness of 10 mm was used in the simulation (Huang et al. 2009). Moreover, the thickness of the simulated coal seam was 8 m, the dip angle of the fault was 50°, and the fall height of the fault was 4 m, which was categorized as a small fall height.

After 7 days of drying, the model could be viewed, and then the plans of displacement and stress monitoring were designed. Among them, 16 monitoring lines were set up, and the 9th and 16th lines were marked as D9 and D16 and chosen to study the displacement variation by using Electronic Total Station; meanwhile, 35 stress sensors were applied to study stress variations by connecting to a DH3815N stress–strain testing system. Figures 2 and 3 show the overview and monitoring plans of physical model.

Results of physical simulation test

Mining process

Before mining, a coal pillar with a width of 150 mm was left at the open-off cut side to eliminate the boundary effect. Subsequently, a 50 mm step increment was synchronously mined from the front and rear of the model, and the interval time between two steps was set to 2 h. Figure 4 depicts the typical states of overlying strata during the process of model mining. Note that all the length parameters are converted into an in situ scale.

When the distance between the working face and the fault exceeded 40 m, it could be defined as $L \geq 40$ m. A typical saddle-shaped fracture pattern of overlying strata formed with $L = 40$ m, as shown in Fig. 4a. At present, the fault is not affected by mining operations, and the overlying structure evolves conventionally.

In Fig. 4b, the fault is beginning to be activated because the high-located strata have rotated, and the fault plane opened due to fault cutting; the maximum and minimum heights of the fault opening fracture (FOF) were 130 and 83 m, respectively. Moreover, the maximum height of the FOF was higher than the maximum height of bed separation (122 m), which further indicates the fault can result in more severe failure. Then, the fault activation was enhanced (Figs. 4c and d), resulting in FOF expansion; maximum and minimum heights were 174 m and 38 m, respectively, and the fracture height of the footwall strata increased to 165 m with $L = 10$ m. With the face continuing to advance, the fault opened completely, as shown in Fig. 4e, because of the sudden roof subsidence; the hanging wall strata rotated and slipped along the fault, which resulted in the high-located FOF reduction. Referring to Fig. 4f, when the face passed through the fault with $L = -30$ m, the cantilevered main roof rotated and was cut down, which resulted in the fracture height in the hanging wall increasing to 69 m. Then, the hanging wall strata slipped, driven by fault cutting and overburden pressure (as shown in Fig. 4g), and the FOF tended to be close; the fracture height footwall strata increased to 178 m due to the hanging wall slipping.

As shown in Fig. 4h, the caved rocks in the hanging wall formed a support structure for overlying strata, which resulted in little effect of the fault on strata movement. The footwall strata moved fully, and the FOF basically closed.

Table 1 Lithology and physical mechanical parameters of roof–floor strata (Wang et al. 2017)

| Lithology	Density		Compression strength		Elastic modulus		Material ratio
	Prototype (kg·m^{-3})	Model (kg·m^{-3})	Prototype (MPa)	Model (kPa)	Prototype (GPa)	Model (MPa)	
Siltstone	2400	1600	27.60	92.00	4.56	15.20	755
Packsand	2400	1600	31.50	105.00	5.04	16.80	782
Gritstone	2400	1600	36.00	120.00	4.86	16.20	773
Coal	2400	1600	16.00	53.30	2.34	7.80	864
Mudstone	2250	1500	17.20	57.40	2.94	9.80	864
Sandy mudstone	2250	1500	21.10	70.30	2.94	9.80	864
Silty mudstone	2250	1500	17.20	57.40	2.94	9.80	864
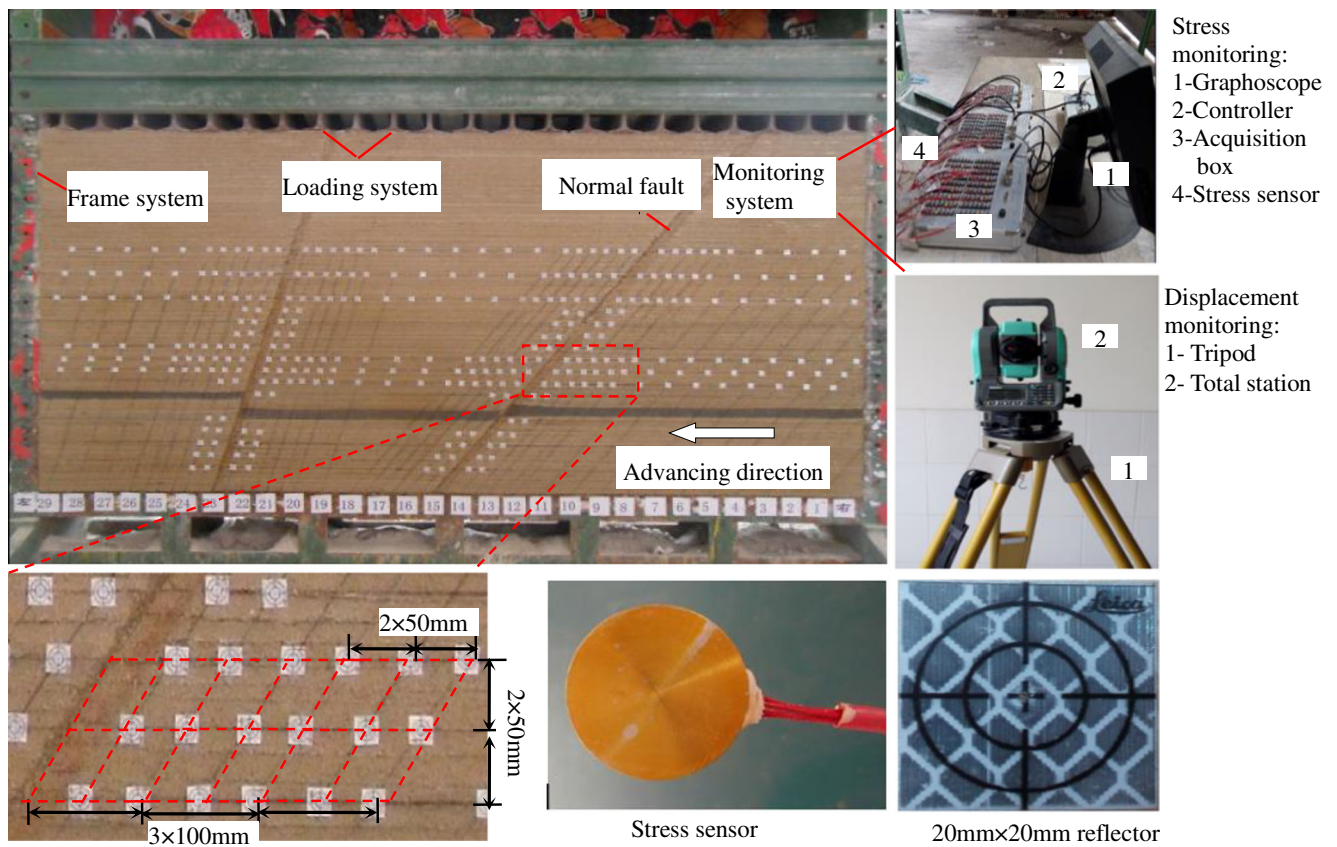
Fig. 2 Physical model and test system (Wang et al. 2017)

Movement characteristics

Figure 5 depicts the movement characteristics of overlying strata at different layers to explain the mining effect affected by a fault quantificationally.

When $L \geq 30$ m, the footwall high-located strata initially rotated to the fault, resulting in the displacement of D16 increasing, with a maximum value of 2.8 m; however, the low-located stratum movement was not affected by the fault, and the maximum displacement value was 5.8 m. When $30 > L \geq$ 10 m, the high-location fault activation aggravated, and the strata slipped prominently, which resulted in the displacement of D16 sharply increasing to 5 m; meanwhile, the low-location fault started to activate, and the displacement of D9 slightly increased to 6.2 m. When $10 > L \geq -30$ m, the hanging wall high-located strata rotated to the fault, and its maximum value of D16 increased to 1.2 m; however, the displacement of D9 in the hanging wall increased sharply because of the main roof cutting down with $L = -30$ m. When $-30 > L \geq -70$ m, the subsidence range expanded, and displacements of D9 and
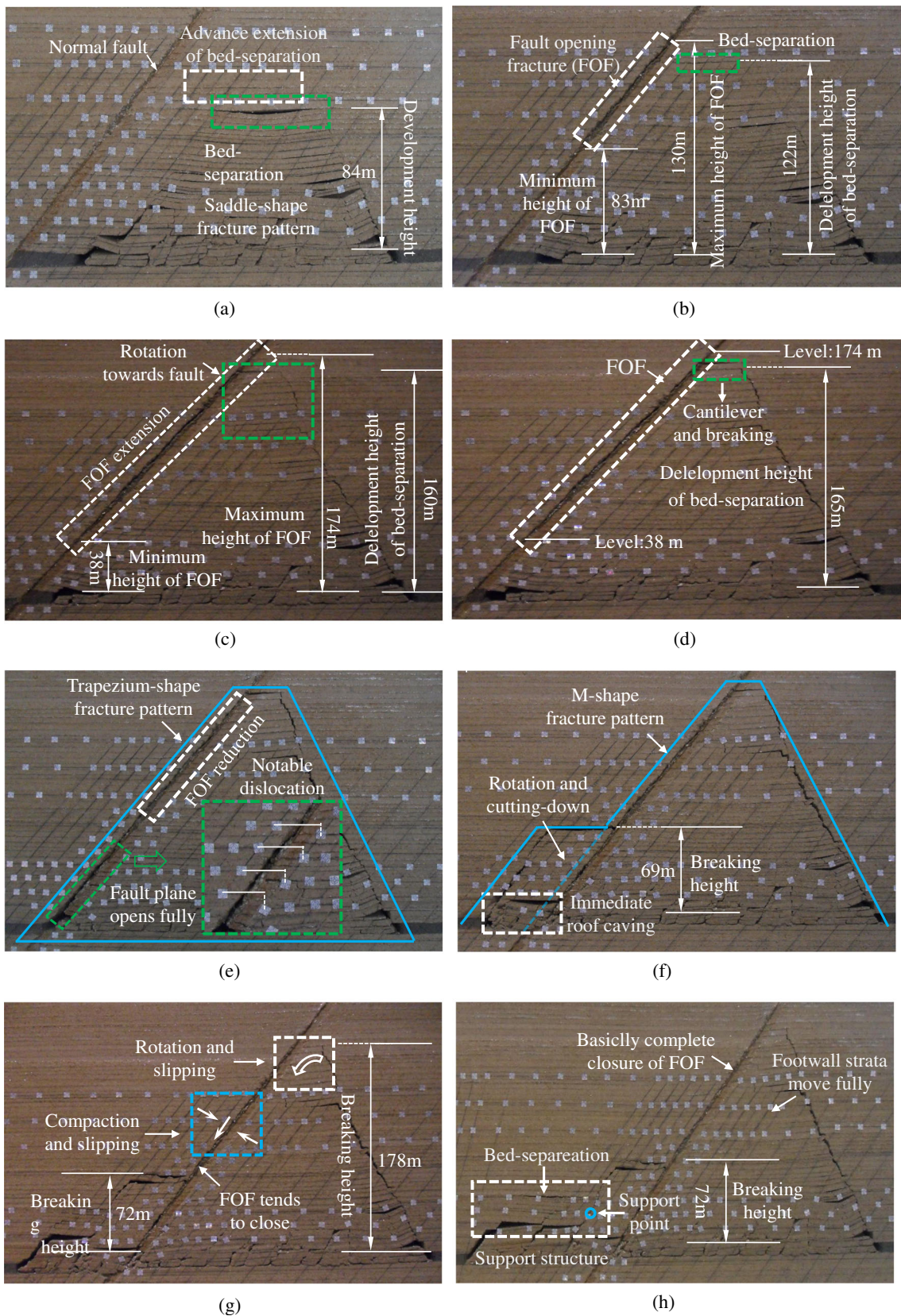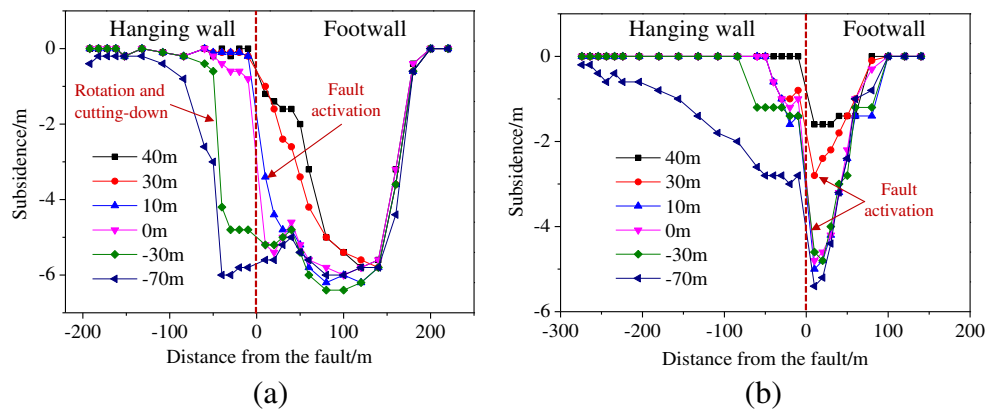
Fig. 3 Plans of displacement and stress monitoring
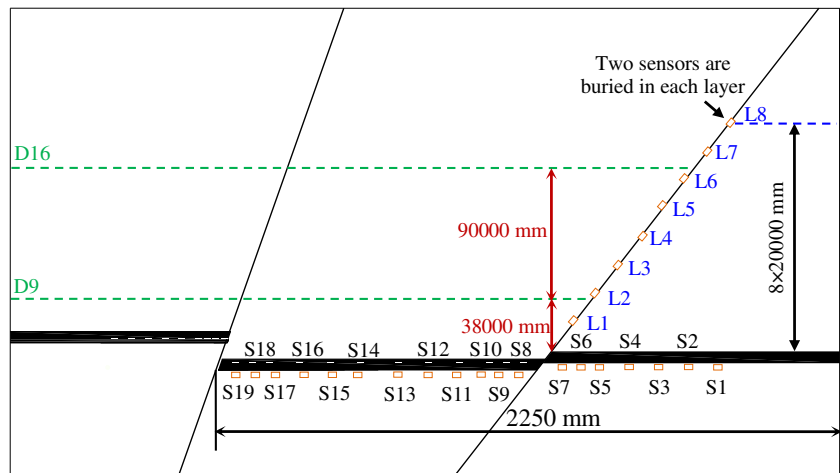
Fig. 4 Movement and structure of overlying strata with a fault occurrence: **a** $L = 40$ m; **b** $L = 30$ m; **c** $L = 20$ m; **d** $L = 10$ m; **e** $L = 0$ m; **f** $L = -30$ m; **g** $L = -70$ m; **h** $L = -110$ m

Fig. 5 Displacement of overlying strata at different layers: **a** D9 monitoring line; **b** D16 monitoring line

(a)   (b)

D16 increased continuously; meanwhile, the displacement of D16 in the hanging wall notably increased to 3 m, while that of footwall increased slightly to 5.4 m, due to the rotation and slipping of hanging wall strata.

Analysis of fault slipping

The displacement of two monitoring lines on two fault walls parallel to the fault plane was monitored. Then, the curve variations of relative displacement (which can represent the fault slipping) were depicted as shown in Fig. 6.

In Fig. 6a, when $L \geq 10$ m, the mining effect on the fault aggravated gradually, and the footwall high-located strata rotated toward the fault, resulting in displacement of the footwall monitoring line being reduced downwards. When $L = 0$ m, the relative displacement increased sharply at the low location because of the sudden strata subsidence. When $0 > L \geq -70$ m, it reduced notably at the low location and aggravated gradually, because of fault activation and hanging wall lower-located strata cutting-down.

Figure 6b shows the displacement variations of two points in the D9 monitoring line of two fault walls. It can be seen that when $L \geq 40$ m, the mining effect on fault was slight, and fault slipping was small. Then, as the fault activation was enhanced, the displacement of footwall strata notably increased to 5.2 m with $40 > L \geq 0$ m, while that of the hanging wall only
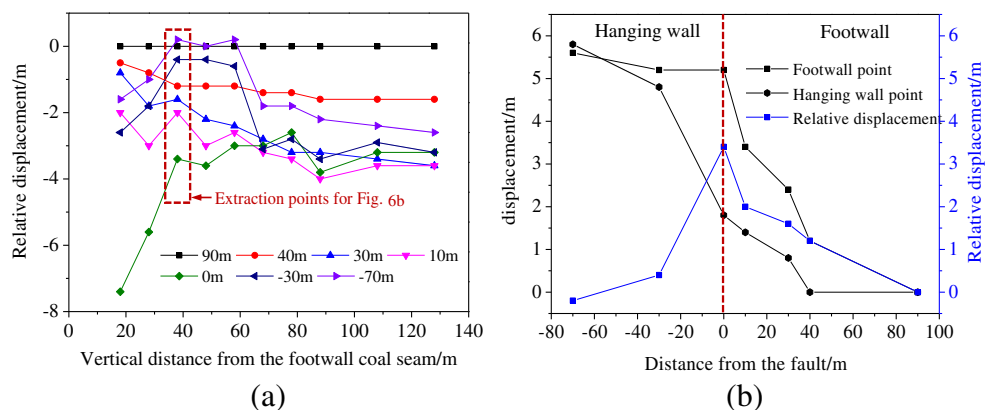
increased to 1.8 m, resulting in the relative displacement sharply increasing, with the peak value of 3.4 m. When $0 > L \geq -30$ m, mining operations had a large effect on the hanging wall strata, and the displacement notably increased to 5.8 m, while it had little effect on the footwall strata and the displacement there displayed no significant change; hence, the relative displacement clearly dropped to 0.4 m with $L = -30$ m. As the face continued to advance, the mining effect on the fault weakened, and the change of fault slipping was not clear.

Stress evolution of fault plane

According to the monitoring scheme of the physical test, the stress data of sensors marked as S23 (L2), S27 (L4) and S31 (L6) were analyzed. Then, the variation curves of normal stress for the fault plane were obtained, as shown in Fig. 7. In the model test, all stress sensors had to be reset to 0 before coal mining. Hence, the positive stress readings from the sensor represent the stress concentration, and this range can be defined as the stress-increased zone, while the negative stress sensor readings depict the stress relief, and this range is defined as the stress-relaxed zone.

As shown in Fig. 7, the normal stress of the fault plane at different layers had different variation characteristics. At the initial stages of mining, the fault is not affected by mining

Fig. 6 Variation of relative displacement of two fault walls: **a** relative displacement of two monitoring lines; **b** displacement of two monitoring points
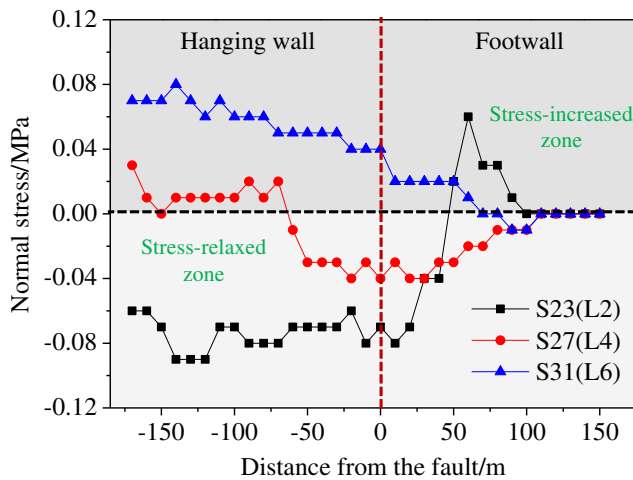

(a)   (b)

Fig. 7 Variation curves of normal stress for fault plane

Table 2 Lithologies and thicknesses of the coal and rock mass (Chen et al. 2016)

Sequence	Lithology	Thickness (m)
Main roof	Medium fine sandstone	15.5~18.9
Immediate roof	Siltstone	3.4~5.4
Coal seam	Coal	8.6~8.9
Immediate floor	Siltstone	3.6~4.6
Main floor	Medium fine sandstone	16.4~18.3

activation; hence, the normal stress of the fault plane remained unchanged. As the face advanced toward the fault, only S27 and S31 at the high position were affected by mining disturbance, and both normal stresses were − 0.01 MPa. Then, the effect of fault activation was enhanced and the fault plane opened, resulting in the stress of S27 dropping to − 0.04 MPa; however, the stress of S31 recovered and increased, gradually affected by compaction of the hanging wall strata. Moreover, the stress of S23 increased to 0.06 MPa and then dropped sharply because of fault plane opening. Finally, the increased stress of S27 was clearly due to hanging wall strata rotation, which then tended to stabilize.

Abutment stress evolution of coal body

Six sensors, marked as S2, S5, S7, S9, S11, and S14 at the floor strata, were chosen to study the effect of fault activation slipping on abutment stress of the coal body. Among them, S2 and S5 were at the footwall and far from the fault, at 84 m and 30 m, respectively; S7 was near the fault and far from the fault,
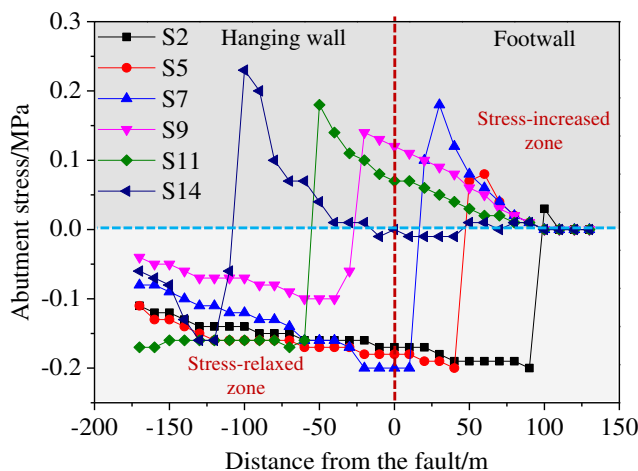
at 10 m in footwall; and S9, S11, and S14 were at the hanging wall and far from the fault at 20 m, 48 m, and 106 m, respectively.

As shown in Fig. 8, when the face approached the monitoring points, the abutment stress concentrated in S2 and S5, and gradually increased to a peak value. For instance, the peak stress of S5 was 0.08 MPa, and then dropped sharply; after that, it recovered as the caving rocks compacted, but it was still smaller than that of in situ stress. When the face approached the fault, the abutment stress at S7 increased notably with a peak value of 0.18 MPa, because of fault coal pillar reduction and fault activation. This value was 2.25 times the peak stress of S5, and greater than that of the non-affected zone. When the face just passed through the fault, the fault still activated, and the hanging wall strata rotated and slipped, which resulted in the abutment stress of S9 and S11 increasing. With the face continuing to advance, a stable structure was formed (as shown in Fig. 4); a high abutment stress was displayed at S14 with a peak value of 0.23 MPa, which was 2.88 times the peak stress of S5.

Hence, it can be concluded that prior to passing the fault, the fault is activated from high location to low location, and it aggravates gradually, which leads to increasing abutment stress of the footwall coal. After passing the fault, the cutting-down strata are compacted and slipped, which can result in the abutment stress of the hanging wall coal increasing; however, the hanging wall strata move slightly, and the displacement is smaller compared to that of the footwall. The fault is activated and slips in the range of − 70 to 30 m, in which rock bursts are easily induced.

Analysis of field observation

Geological conditions

In this section, panel 14310 of Dongtan coalmine in Shandong province (as shown in Fig. 9) is taken as the study background of field observation. The mining depth and thickness of coal seam are 600 m and 8.2 m, and the length of the face 262.9 m. The thicknesses and

Fig. 8 Variation curves of abutment stress of coal body

Fig. 9 Plan of panel 14310
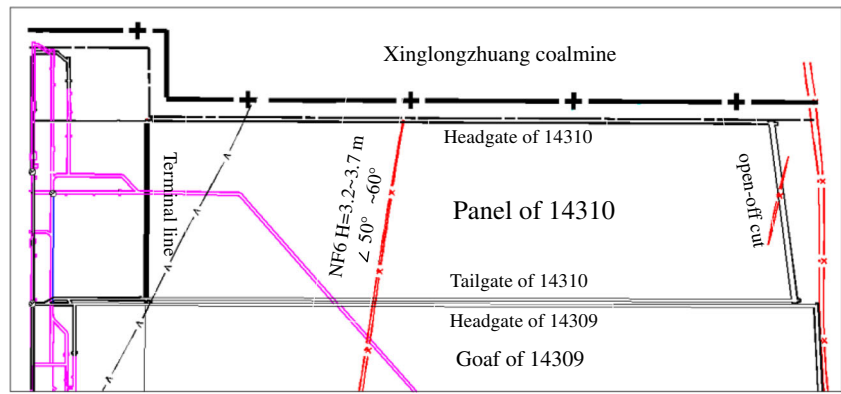
lithologies of the panel strata are listed in Table 2 according to the borehole histogram of No.49. Based on the field report, a normal fault marked as NF6 is located in the middle of face, which has a notable effect on mining of panel 14310.

Analysis of field observation

To study the mining effect in the field, microseismic events were monitored by a seismological observation system (SOS), which was installed in May 2010 in Dongtan coalmine (Bischoff et al. 2010; Sainoki and Mitri 2014). Figure 10 shows the distributions of microseismic activities during the period from July 26, 2010, to August 25, 2010; herein, the shapes represent different energy of microseismic events, and

these positions represent the locations of microseismic events. Figure 11 depicts variation of total counts and total energy for the microseismic events per day during the period from July 11, 2010, to August 28, 2010.

During face mining before July 24, it was far away from the fault, exceeding 62 m; the fault was slightly affected by mining, and the microseismic events were mainly distributed in front of the coal wall and near the goaf. The total energy and total counts of microseismic events were very low, as shown in Fig. 11 for stage I, where the pressure appearance from the field observation is similar to the simulation results with $L \geq$ 40 m in section "Mining process."

During the period from July 25 to August 2, the face was far away from the fault, at approximately 40 m; the counts of microseismic events increased and concentrated
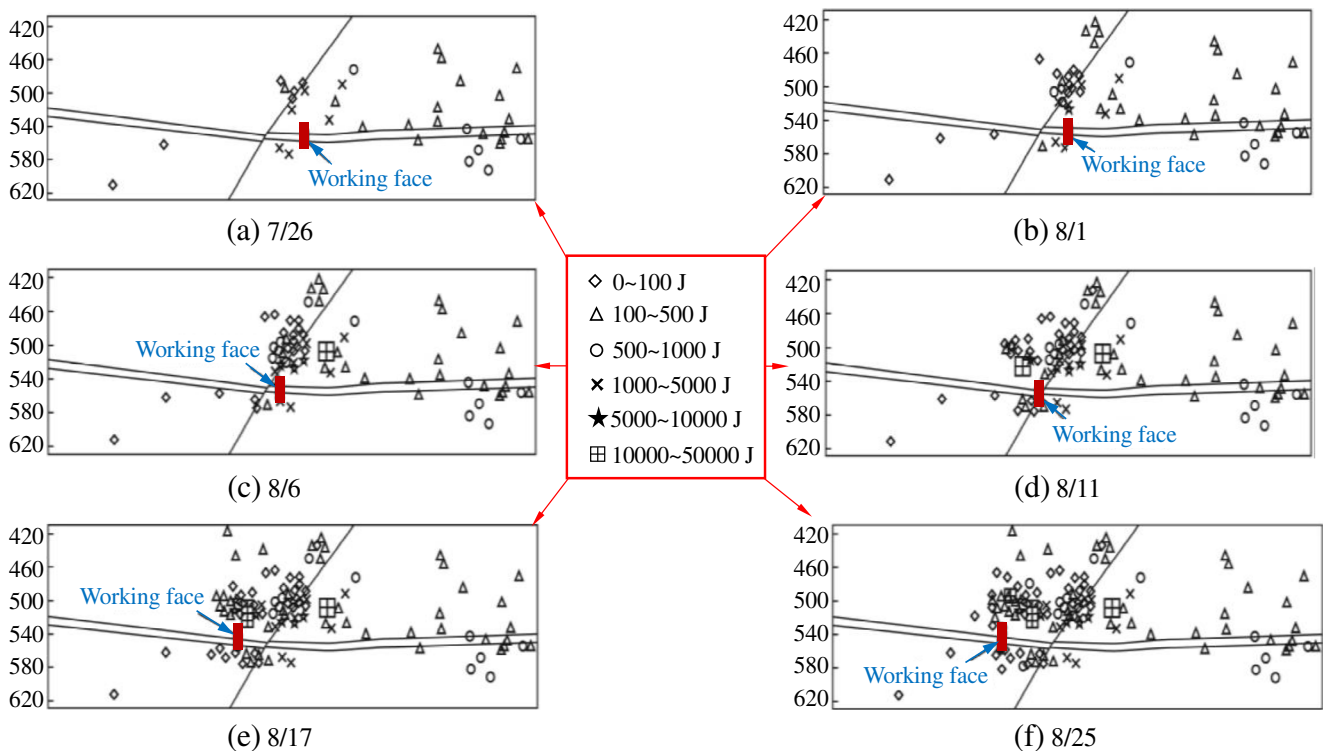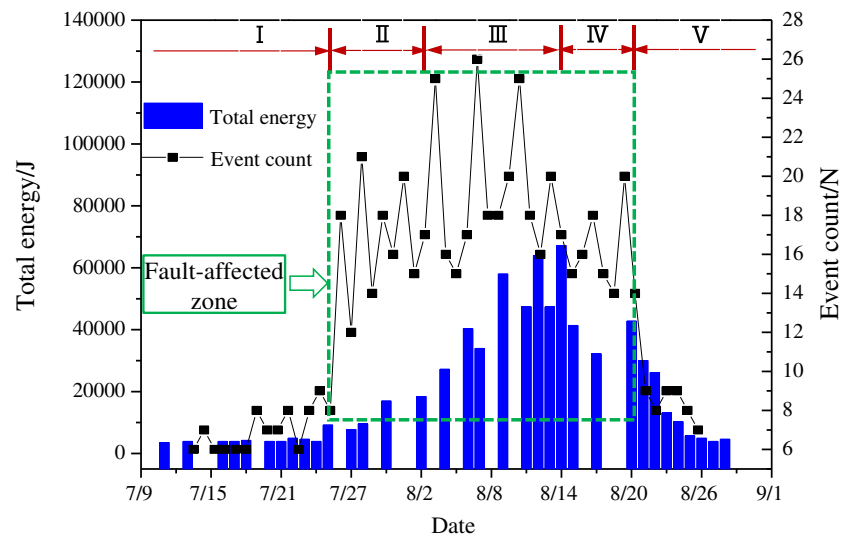

Fig. 10 Sectional distribution of microseismic events (Chen et al. 2016): **a** July 26; **b** August 1; **c** August 6; **d** August 11; **e** August 17; **f** August 25

Fig. 11 Energy and counts of microseismic events between July 11, 2010, and August 28, 2010

near the fault, as shown in Fig. 10a and b. This indicates that the fault begins to be affected by mining and aggravates gradually. However, the total energy did not change considerably, with mainly small energies (less than 5000 J), as shown in Fig. 11 with stage II. At this stage, the pressure appearance of field observations is similar to the simulation results with $40 > L \geq 10$ m in section "Mining process."

In Fig. 10c and d, during the period from August 3 to August 14, the face passed through the fault approximately 24 m, and the counts of microseismic events increased notably due to violent fault activation and slipping, resulting in the total counts and total energy increasing sharply and rising to a peak, as shown in Fig. 11 for stage III. Moreover, several microseismic events with large energy (10,000–50,000 J) occurred near the fault. Hence, the pressure appearance of field observation is similar to the simulation results with $10 > L \geq -30$ m in section "Mining process."

During the period from August 15 to August 22, the face passed through the fault by approximately 68 m, and the distribution of microseismic events in the footwall did not change, while in the hanging wall they moved forward, as shown in Fig. 10e. Moreover, the total counts and total energy notably dropped and aggravated gradually, as shown in Fig. 11 for stage IV. This indicates that the mining effect on faults weakens, and the fault activation effect decreases, which is similar to the simulation results with $-30 > L \geq -70$ m in section "Mining process."

When the face passes through the fault exceeding 68 m after August 22, the microseismic events are no longer affected by the fault, and they redistribute in front of the coal wall and near the goaf, as shown in Fig. 10f. Moreover, the large-energy microseismic events also no longer occur, and the total counts and total energy drop and retain this low level, as shown in Fig. 11 for stage V. The pressure appearance of field

observation at this stage is similar to the simulation results with $L < -70$ m in section "Mining process."

Hence, regarding mining effects caused by a fault tectonic, comparing the results of field observations and physical simulations, the results between these two methods display good agreement, which verifies the correctness and feasibility of the physical model test and its simulation results. Moreover, this also reflects the advantages of physical simulation, such as the ability to reconstruct phenomena that cannot be directly observed in the field.

Conclusions

In this study, a physical simulation test simulating a progressive mining operation with a fault occurrence was performed. The mining effect on fault activation slipping, the responses of abutment stress of coal body, and fault plane stress during the fault slipping process were studied and analyzed. We can obtain several conclusions as follows.

- Prior to passing the fault, it is activated from high location to low location, and it aggravates gradually, which leads to the abutment stress of footwall coal increasing; moreover, the footwall strata move fully, and the displacement is large.
- After just passing the fault, the cutting-down strata are compacted and slip along fault plane, which can exert load on the hanging wall coal and lead to increasing abutment stress of the hanging wall coal; however, the hanging wall strata move slightly, and the displacement is small compared to the footwall.
- The fault is activated and slips in the range of -70 to 30 m in this paper, and the slipping mutation of two fault walls occurs successively, which can easily induce rock bursts

near the fault (the symbol "−" means the face has passed through the fault).

Finally, a field case regarding microseismic monitoring was used to verify the simulation results.

Study results can serve as a reference for predicting rock bursts and their classification into hazardous areas under similar conditions.

References

Bischoff M, Cete A, Fritschen R, Meier T (2010) Coal mining induced seismicity in the Ruhr area, Germany. Pure Appl Geophys 167:63–75

Bornyakov SA, Panteleev IA, Tarasova AA (2016) Dynamics of intrafault deformation waves: results of physical simulation. Dokl Earth Sci 471:1316–1318

Chen XH, Lyu PF, Song WH, Deng CS (2016) Analysis and control technology of danger of rock burst when fully mechanized caving passing through fault. China Safety Sci J 26:81–87 (in Chinese)

Dai HY, Lian XG, Liu JY, Liu YX, Zhou YM, Deng WN, Cai YF (2010) Model study of deformation induced by fully mechanized caving below a thick loess layer. Int J Rock Mech Min Sci 47:1027–1033

Dou ZS, Wu JW, Wang L, Zhai XR, Li WQ, Lu L, Ma YZ (2017) Similar physical simulation on the deformation of surrounding rocks of floor roadway caused by coal mining under tectonic stress. J Eng Sci Technol Rev 10:132–140

Gong W, Peng YY, Wang H, He MC, Sousa L (2015) Fracture angle analysis of rock burst faulting planes based on true-triaxial experiment. Rock Mech Rock Eng 48:1017–1039

He J, Jing CS, Chen XS, Jing FX (2010) Numerical simulation research on stress distribution of coal bed fault structure formation and evolution. J Henan Polytechn Univ (Natural Science) 29:1–6 (in Chinese)

Huang BX, Liu CY, Xu JL (2009) Effect of little fault in working face on water conducted fissure height. J China Coal Soc 34:1316–1321 (in Chinese)

Jiang YD, Wang T, Zhao YX, Wang WJ (2013) Experimental study on the mechanisms of fault reactivation and coal bumps induced by mining. J Coal Sci Eng 19:507–513 (in Chinese)

Jiang LS, Wang P, Zhang PP, Zheng PP, Xu B (2017) Numerical analysis of the effects induced by normal faults and dip angles on rock bursts. Compte Rendu Mecanique 345:690–705

Jiang JQ, Wang P, Jiang LS, Zheng PQ, Feng F (2018) Numerical simulation on mining effect influenced by a normal fault and its induced effect on rock burst. Geomech Eng 14:337–344

Lai XP, Shan PF, Cao JT, Cui F, Sun H (2016) Simulation of asymmetric destabilization of mine-void rock masses using a large 3D physical model. Rock Mech Rock Eng 49:487–502

Li, H. C. 1988. Similar simulation test for ground pressure. China Univ Min Technol Press, Xuzhou, pp. 103(in Chinese)

Li ZH, Dou LM, Lu CP, Mou ZL, Cao AY (2008) Study on fault induced rock bursts. Int J Min Sci Technol 18:321–326

Li ZL, Dou LM, Cai W, Wang GF, Jiang H, Ding YL, Kong Y (2016) Mechanical analysis of static stress within fault-pillars based on a voussoir beam structure. Rock Mech Rock Eng 49:1097–1105

Liu YK, Zhou FB, Liu L, Liu C, Hu SY (2011) An experimental and numerical investigation on the deformation of overlying coal seams above double seam extraction for controlling coal mine methane emissions. Int J Coal Geol 87:139–149

Peng JB, Chen LW, Huang QB, Men YM, Fan W, Yan JK (2013) Physical simulation of ground fissures triggered by underground fault activity. Eng Geol 155:19–30

Sainoki A, Mitri HS (2014) Methodology for the interpretation of fault-slip seismicity in a weak shear zone. J Appl Geophys 110:126–134

Sainoki A, Mitri HS (2015) Effect of slip-weakening distance on selected seismic source parameters of mining-induced fault-slip. Int J Rock Mech Min Sci 73:115–122

Sherizadeh T, Kulatilake PHSW (2016) Assessment of roof stability in a room and pillar coal mine in the U.S. using three-dimensional distinct element method. Tunn Undergr Space Technol 59:24–37

Shreedharan S, Kulatilake PHSW (2016) Discontinuum-equivalent continuum analysis of the stability of tunnels in a deep coal mine using the distinct element method. Rock Mech Rock Eng 49:1903–1922

Wang AW, Pan YS, Li ZH, Liu CS, Han RJ, Lv XF, Lu HQ (2014a) Similar experimental study of rock burst induced by mining deep coal seam under fault action. Rock Soil Mech 35:2486–2492 (in Chinese)

Wang T, Wang ZH, Jiang YD, Wang WJ (2014b) Experimental study of stress distribution and evolution of surrounding rock under the influence of fault slip induced by mining. J China Univ Min Technol 43:587–592 (in Chinese)

Wang W, Cheng YP, Wang HF, Liu HY, Wang L, Li W, Jiang JY (2015a) Fracture failure analysis of hard-thick sandstone roof and its controlling effect on gas emission in underground ultrathick coal extraction. Eng Fail Anal 54:150–162

Wang C, Zhang NC, Han YF, Qian DY (2015b) Experiment research on overburden mining-induced fracture evolution and its fractal characteristics in ascending mining. Arab J Geosci 8:13–21

Wang P, Jiang JQ, Zhang PP, Wu QL (2016) Breaking process and mining stress evolution characteristics of a high-position hard and thick stratum. Int J Min Sci Technol 26:563–569

Wang P, Jiang LS, Zheng PQ (2017) Application of equivalent materials to modeling fractures in the vicinity of a normal fault in the area of mining exploitation influence. Acta Geodyn Geomater 14:475–485

Wang P, Jiang LS, Jiang JQ, Zheng PQ, Li W (2018) Strata behaviors and rock burst–inducing mechanism under the coupling effect of a hard, thick stratum and a normal fault. Int J Geomech 18:04017135

Wu JW, Tong HS, Tong SJ, Tang DQ (2007) Study on similar material for simulation of mining effect of rock mass at fault zone. Chin J Rock Mech Eng 26:4170–4175 (in Chinese)

Xia YX, Wang JH, Mao DB (2016) Analysis of fault activation induced rock burst risk based on in-situ stress measurements. J China Coal Soc 41:3008–3015

Xia BW, Jia JL, Yu B, Zhang X, Li XL (2017) Coupling effects of coal pillars of thick coal seams in large-space stopes and hard stratum on mine pressure. Int J Min Sci Technol 27:965–972

Xie J, Zhu W, Xu JL, Wen JH, Liu CZ (2016) A study on the bearing effect of pier column backfilling in the goaf of a thin coal seam. Geosci J 20:361–369

Xing Y, Kulatilake PHSW, Sandbak LA (2018a) Investigation of rock mass stability around the tunnels in an underground mine in USA using three-dimensional discontinuum numerical modeling. Rock Mech Rock Eng 51:579–597

Xing Y, Kulatilake PHSW, Sandbak LA (2018b) Effect of rock mass and discontinuity mechanical properties and delayed rock supporting on tunnel stability in an underground mine in USA. Eng Geol 238:62–75

Xuan DY, Xu JL (2017) Longwall surface subsidence control by technology of isolated overburden grout injection. Int J Min Sci Technol 27: 813–818

Zhang SC, Guo WJ, Sun WB, Li YY, Wang HL (2015) Experimental research on extended activation and water inrush of concealed structure in deep mining. Rock Soil Mech 36:3111–3120 (in Chinese)

Zhang SC, Guo WJ, Li YY, Sun WB, Yin DW (2017) Experimental simulation of fault water inrush channel evolution in a coal mine floor. Mine Water Environ 36:443–451

Zuo JP, Chen ZH, Wang HW, Liu XP, Wu ZP (2009) Experimental investigation on fault activation pattern under deep mining. J China Coal Soc 34:305–309 (in Chinese)